Exciton Structure and Magneto-Optical Effects in ZnS*†‡

JOHN C. MIKLOSZ AND ROBERT G. WHEELER
Yale University, New Haven, Connecticut

(Received 11 June 1965; revised manuscript received 20 July 1966)

The exciton structure in hexagonal ZnS has been studied in transmission and interpreted in terms of an effective-mass formalism. The $n_1=1, 2, 3, 4$, and 5 states of the first ($\Gamma_7-\Gamma_9$) series, and the $n_2=1,2$, and 3 states of the second ($\Gamma_7-\Gamma_7$) series have been observed and identified. From the series limits, a band gap of 31 543 cm^{-1} and a crystal-field splitting of $\approx$240 cm^{-1} has been measured. Using a semiempirical theory of exciton structure to interpret the behavior of the excited states in the presence of an external magnetic field, band parameters for the Γ_7 conduction band and the Γ_9 valence band have been obtained. We find an isotropic electron effective mass $m_e=0.28\pm0.03$, and an anisotropic hole mass with $m_{hx}=0.49\pm0.06$, $m_{hz}=1.4$, where m_e and m_h are expressed in terms of the free-electron mass. In addition, the conduction-band electron is found to have a g value approximately equal to 2. The most interesting feature of the exciton spectra is that interpretation of the first-series excited states requires the assignment of so-called forbidden symmetry. It is shown that the occurrence of very strong forbidden transitions in ZnS is in line with the trend exhibited by the exciton spectra of CdSe and CdS.

INTRODUCTION

THE existence of exciton spectra and magneto-optical effects in the Group II–VI compounds provides a method for investigating the band structure of these materials in great detail. Exciton ground states for the three series derived from the single S-like conduction band and the three P-like valence bands in ZnS have been observed in reflection by Birman *et al.*[1] In transmission, Piper *et al.*[2] was able to observe the $n=1$ states of both the first and third series and the $n=1,2$ states of the second series. This is to report on the observation of higher excited states of both the first and second series and the detailed behavior of the first series in the presence of an external magnetic field, since these states are sufficiently narrow to provide meaningful results. A quantitative comparison of the observed energies of the $2S$, $2P_{\pm1}$, and $3D_{\pm1,\pm2}$ states of the first series with an anisotropic-exciton-mass formalism allows the evaluation of the electron and hole masses and g-value parameters.[3] In addition, several exciton states are observed when the magnetic energy is an order of magnitude greater than the Coulomb binding energy for the states. Comparison of these energies with a high-field approximation[4,5] corroborates the band parameters obtained from the low-lying exciton states.

An effective-mass formalism may be used to describe the experimental situation if the following assumptions characterize the electronic band structure of ZnS:

(1) The band extrema are at or very near $\mathbf{k}=0$, so that the energy surfaces may be considered ellipsoidal and the electron and hole masses expressed as diagonal tensors. Casella[6] has shown that the secular determinant defining the energy surfaces of a Γ_7 conduction band may contain off-diagonal terms linear in $\mathbf{k}$. These terms are quite small however and may be neglected to a first approximation.

(2) The exciton-mass anisotropy and the dielectric anisotropy are small, allowing first-order perturbation calculations to be made for the exciton energy states and magnetic field effects.

(3) The energy of the longitudinal optical phonon is much greater than the exciton binding energy, allowing low-frequency dielectric constants to be used with no corrections for polaron effects. This is expected to be the case for exciton states with $n=3$ and above which have small binding energies and large orbital radii.

(4) The valence-band splittings are large compared to the binding energies of the exciton states allowing one to neglect mixing between valence bands.

While the first three conditions are believed to hold for ZnS, there is some question as to the validity of neglecting the interband mixing. This mixing has been estimated to be proportional to[7,8]

$$(R/\Delta E)a/a_0^*,$$

where R is the exciton binding energy, ΔE the interband separation, a the lattice constant, and a_0^* the exciton Bohr radius. As we shall see, $R\approx250$ cm^{-1} and $a_0^*\approx25$ Å for the first-series exciton in ZnS. Using the crystal-field splitting of $\approx$240 cm^{-1} determined for the two uppermost valence bands, we find a value of ≈0.2 for the

* Supported in part by the Office of Scientific Research, U. S. Air Force.

† Based on a thesis presented to the faculty of the Graduate School of Yale University in partial fulfillment of the requirements for the Ph.D. degree by John C. Miklosz.

‡ A preliminary report of this work is to be found in the *Proceedings of the 7th International Conference on the Physics of Semiconductors, Paris*, 1964 (Academic Press Inc., New York, 1964). Therein the symmetry of some lines are incorrectly identified.

[1] J. L. Birman, H. Samelson, and A. Lempicki, G T & E Res. Develop. J. **1**, 2 (1961).

[2] W. W. Piper, P. D. Johnson, and D. T. F. Marple, J. Phys. Chem. Solids **8**, 457 (1959).

[3] R. G. Wheeler and J. O. Dimmock, Phys. Rev. **125**, 1805 (1962).

[4] R. J. Elliot and R. Loudon, J. Phys. Chem. Solids **8**, 382 (1959).

[5] R. J. Elliot and R. Loudon, J. Phys. Chem. Solids **15**, 196 (1960).

[6] R. C. Casella, Phys. Rev. Letters **5**, 371 (1960).

[7] J. O. Dimmock, *Semiconductors and Semimetals* (Academic Press Inc., New York, to be published), Chap. 3.6.

[8] W. Kohn, Solid State Phys. **5**, 257 (1957).

TABLE I. Energies for $\mathbf{H}\|C$: first series, $n_1=1,2,3$.

State	C_{6v}	Energy[a]
$1S$	Γ_5	$E_1^0\left(1+\frac{1}{3}\alpha+\frac{3}{20}\alpha^2\right)+\sigma H_z^2\pm\frac{1}{2}(g_{hz}-g_{ez})\beta_0 H_z$
$2S$	Γ_5	$E_2^0\left(1+\frac{1}{3}\alpha+\frac{3}{20}\alpha^2\right)+14\sigma H_z^2\pm\frac{1}{2}(g_{hz}-g_{ez})\beta_0 H_z$
$2P_0$	Γ_5	$E_2^0\left(1+\frac{3}{5}\alpha+\frac{9}{28}\alpha^2\right)+6\sigma H_z^2\pm\frac{1}{2}(g_{hz}-g_{ez})\beta_0 H_z$
$2P_{\pm1}$	$\Gamma_1+\Gamma_2$	$E_2^0\left(1+\frac{1}{5}\alpha+\frac{9}{140}\alpha^2\right)+12\sigma H_z^2\pm\left[\frac{1}{\Delta_x}-\frac{1}{2}(g_{hz}-g_{ez})\right]\beta_0 H_z$
$2P_{\pm1}$	Γ_5	$E_2^0\left(1+\frac{1}{5}\alpha+\frac{9}{140}\alpha^2\right)+12\sigma H_z^2\pm\left[\frac{1}{\Delta_x}-\frac{1}{2}(g_{hz}+g_{ez})\right]\beta_0 H_z$
$3S$	Γ_5	$E_3^0\left(1+\frac{1}{3}\alpha+\frac{3}{20}\alpha^2\right)+69\sigma H_z^2\pm\frac{1}{2}(g_{hz}-g_{ez})\beta_0 H_z$
$3P_0$	Γ_5	$E_3^0\left(1+\frac{3}{5}\alpha+\frac{9}{28}\alpha^2\right)+36\sigma H_z^2\pm\frac{1}{2}(g_{hz}-g_{ez})\beta_0 H_z$
$3P_{\pm1}$	$\Gamma_1+\Gamma_2$	$E_3^0\left(1+\frac{1}{5}\alpha+\frac{9}{140}\alpha^2\right)+72\sigma H_z^2\pm\left[\frac{1}{\Delta_x}-\frac{1}{2}(g_{hz}-g_{ez})\right]\beta_0 H_z$
$3D_0$	Γ_5	$E_3^0\left(1+\frac{11}{21}\alpha+\frac{9}{28}\alpha^2\right)+30\sigma H_z^2\pm\frac{1}{2}(g_{hz}-g_{ez})\beta_0 H_z$
$3D_{\pm1}$	$\Gamma_1+\Gamma_2$	$E_3^0\left(1+\frac{3}{7}\alpha+\frac{5}{28}\alpha^2\right)+36\sigma H_z^2\pm\left[\frac{1}{\Delta_x}-\frac{1}{2}(g_{hz}-g_{ez})\right]\beta_0 H_z$
$3D_{\pm1}$	Γ_5	$E_3^0\left(1+\frac{3}{7}\alpha+\frac{5}{28}\alpha^2\right)+36\sigma H_z^2\pm\left[\frac{1}{\Delta_x}-\frac{1}{2}(g_{hz}+g_{ez})\right]\beta_0 H_z$
$3D_{\pm2}$	$\Gamma_1+\Gamma_2$	$E_3^0\left(1+\frac{1}{7}\alpha+\frac{1}{28}\alpha^2\right)+54\sigma H_z^2\pm\left[\frac{2}{\Delta_x}-\frac{1}{2}(g_{hz}+g_{ez})\right]\beta_0 H_z$
$3D_{\pm2}$	Γ_5	$E_3^0\left(1+\frac{1}{7}\alpha+\frac{1}{28}\alpha^2\right)+54\sigma H_z^2\pm\left[\frac{2}{\Delta_x}-\frac{1}{2}(g_{hz}-g_{ez})\right]\beta_0 H_z$

[a] Where $\alpha=\left[1-\frac{\mu_x}{\mu_z}\frac{1}{\eta}\right]$, $\sigma=\frac{1}{4}\frac{e^2}{mc^2}a_0^2\frac{1}{\mu_x^3}\epsilon^2\eta$,
$\frac{1}{\mu_x}=\frac{m}{m_{ex}}+\frac{m}{m_{hx}}$, $\frac{1}{\Delta_x}=\frac{m}{m_{ex}}-\frac{m}{m_{hx}}$.

mixing. Now this should be compared with ≈0.3 as found for CdS and ≈0.05 for CdSe. Since the interpretation of the exciton spectra in CdS yields band parameters in agreement with measurements not related to exciton effects, the interband mixing appears to be negligible at least as far as the band parameters are concerned.

While it may be safe to neglect the interband mixing in the determination of the band parameters, one cannot neglect the effect of this mixing on the selection rules for optical transitions. The occurrence of adjacent valence bands destroys the simple conduction-band–single-valence-band selection rules and gives rise to strong forbidden (wave-vector-dependent) transitions. In the case of CdS[9,10] the forbidden transitions in the polarization $\mathbf{E}\|C$ were stronger than the allowed dipole transitions for the $2P$ states, and as we shall see, a similar situation exists for ZnS.

THEORY

In the ellipsoidal effective-mass approximation the Hamiltonian for an exciton in the presence of an external magnetic field parallel to the crystal C axis ($\mathbf{H}\|C$) may be written as[3,11]

$$\begin{aligned}\mathcal{H}=&\left[-\left(\frac{\hbar^2}{2m}\right)\left\{\frac{1}{\mu_x}\frac{\partial^2}{\partial x^2}+\frac{1}{\mu_x}\frac{\partial^2}{\partial y^2}+\frac{1}{\mu_z}\frac{\partial^2}{\partial z^2}\right\}\right.\\&\left.-\frac{e^2}{\epsilon\eta^{1/2}}\left(x^2+y^2+\frac{\mu_z}{\mu_x}z^2\right)^{-1/2}\right]\\&-\frac{e^2}{\epsilon\eta^{1/2}}\left\{\left(x^2+y^2+\frac{z^2}{\eta}\right)^{-1/2}-\left(x^2+y^2+\frac{\mu_z}{\mu_x}z^2\right)^{-1/2}\right\}\\&+\beta_0\frac{1}{\Delta_x}H_zL_z+\frac{1}{8}\frac{e^2}{mc^2}\frac{1}{\mu_x}H_z^2(x^2+y^2)\\&+\tfrac{1}{2}\beta_0(g_{ez}\sigma_{ez}+g_{hz}\sigma_{hz})H_z,\end{aligned}\tag{1}$$

where m is the free-electron mass and

$$\frac{1}{\mu_\gamma}=m\left(\frac{1}{m_{e\gamma}}+\frac{1}{m_{h\gamma}}\right),\quad\frac{1}{\Delta_\gamma}=m\left(\frac{1}{m_{e\gamma}}-\frac{1}{m_{h\gamma}}\right).\tag{2}$$

Cylindrical symmetry about the crystal C axis, which defines the z direction, is assumed, with ϵ being the dielectric constant normal to z, and $\epsilon\eta$ the dielectric constant along z.

The first term is simply a hydrogen-like Hamiltonian generalized to include mass anisotropy with eigenvalues related to the hydrogenic eigenvalues by

$$\frac{R_{\text{eff}}}{n^2}=\frac{\mu_x}{\epsilon^2\eta}\frac{R_H}{n^2}.\tag{3}$$

Dielectric and exciton-mass anisotropy are also represented by the second term. The effects of this term can be written in terms of an anisotropy constant α, where

$$\alpha=1-(\mu_x/\mu_z)(1/\eta).\tag{4}$$

If the anisotropy is small, this term can be expanded in powers of α and treated as a perturbation. Energies for exciton states with $n_1=1,2,3$ to second order in α are given in Table I.

The third and fourth terms represent the linear and quadratic magnetic field effects and have selection rules

$$\Delta n=0,\quad\Delta l=0,\quad\Delta m=0;$$

and

$$\Delta l=0,\quad\pm2,\quad\Delta m=0.$$

Unlike the linear magnetic field operator, the quadratic field operator is not diagonal in n and hence mixes exciton states of different principal quantum number. For states with $n=3$ and above this mixing is significant, and for very large magnetic fields the treatment of H as a perturbation to the Coulomb interaction breaks down completely.

[9] J. J. Hopfield and D. G. Thomas, Phys. Rev. **122**, 35 (1961).
[10] D. G. Thomas and J. J. Hopfield, Phys. Rev. **124**, 657 (1961).

[11] Reference 9 uses for the analysis of the exciton spectra of CdS a similar theory containing slightly different transformations than used in Ref. 3.

In the geometry $\mathbf{H}\perp C$ the linear magnetic field perturbation can be obtained approximately[3] from the operator

$$H_{\mathrm{LIN}}=\beta_0(a/\Delta_x)H_xL_x, \tag{5}$$

where

$$a=\frac{1}{2}\left(\frac{\mu_z}{\mu_x}\right)^{1/2}\left(\frac{\Delta_x}{\Delta_z}+\frac{\mu_x}{\mu_z}\right) \tag{6}$$

with selection rules $\Delta n=0$, $\Delta l=0$, $\Delta m=\pm 1$. The quadratic perturbation for $\mathbf{H}\perp C$ becomes

$$H_q=\frac{1}{8}\frac{e^2}{mc^2}\frac{1}{\mu_z}H_x^2(y^2+z^2) \tag{7}$$

with selection rules $\Delta l=0, \pm 2$; $\Delta m=0, \pm 2$. As in the $\mathbf{H}\|C$ case, this operator is not diagonal in n.

The first-order energies of observable exciton states of principal quantum number $n_1=1,2,3$ with $\mathbf{H}\|C$ are summarized in Table I. It should be noted that only diagonal energy terms have been included. The effects due to mixing between states of different n will be considered in the discussion of the experimental results. Because the linear operator for $\mathbf{H}\perp C$ is not diagonal in m, one must diagonalize a secular determinant in order to find the energies of the exciton states in a magnetic field, and no simple table analogous to Table I can be made for states with $n=3$ and above in the $\mathbf{H}\perp C$ orientation.

EXPERIMENTAL PROCEDURE

The experiments were performed on zinc sulfide single-crystal platelets of 1–5 μ thickness with the crystal C axis in the plane of the plate, grown by dynamic vapor-phase deposition at $\approx$1100°C from luminescent-grade zinc sulfide powder with argon as a carrier gas. The method is similar to that described by Reynolds,[12] and used successfully for other II–VI compounds. The phase transformation at $\approx$1020°C however makes the growth of pure wurtzite ZnS very sensitive to the deposition temperature, gas flow, etc., and crystals of adequate size and quality for the observation of narrow exciton states are quite rare.

In order to verify the crystal structure and orientation, and obtain some indication of the strains present, the crystals were examined by the single-crystal Laue technique. Only crystals which yielded well-defined Laue patterns were used in the experiments. Crystals which did possess some strain showed inhomogeneous Stark effects in the narrow exciton states. The samples were mounted strain-free and immersed in liquid helium at 1.8°K or lower for all experiments. A concave grating spectrograph in a stigmatic Wadsworth mounting was used in second order with a dispersion of about 2 Å/mm. To obtain sufficient intensity in the ultraviolet, an Osram high-pressure xenon arc lamp was used as a source of continuous radiation. The magnet used was calibrated to 0.1% with current stability of the order of 1 part in 10^5. The spectra were obtained from Kodak type-0 spectrographic plates by a recording densitometer.

[12] D. C. Reynolds, *Art and Science of Growing Crystals* (John Wiley & Sons, Inc., New York, 1963), pp. 62–79.

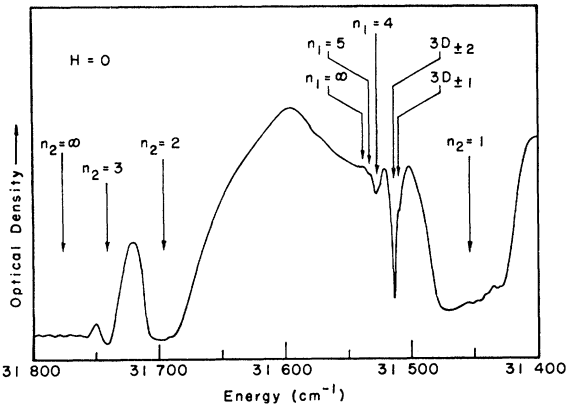

FIG. 1. Absorption spectra of a crystal of about 2 μ thickness with unpolarized radiation. The $n_1=3, 4, 5$ and the $n_2=1, 2, 3$ states are indicated as well as the series limits.

EXPERIMENTAL RESULTS AND INTERPRETATION

A typical absorption spectrum in the vicinity of the second series for a crystal of approximately 2 μ thickness is shown in Fig. 1. The $n_2=1,2$ states are indicated and their energies agree with those observed by Piper *et al.* In addition to $n_2=1,2$ we also observe the $n_2=3$ state. An analysis of the second series will be temporarily postponed and we shall concentrate at present on the first series to which the sharp lines above $n_2=1$ belong. The ground state of the first series has also been seen in the polarization $E\perp C$ but has not been shown.

From a tentative identification of the sharp lines near 31513 cm^{-1} and 31535 cm^{-1} as $n_1=3,4$ states, without regard to any particular orbital assignment, i.e., neglecting the anisotropy, an approximate value for the effective Rydberg for the series can be immediately obtained and one finds $R_{\mathrm{eff}}\approx 250$ cm^{-1}. With this value of the Rydberg, the approximate location of the $n_1=2$ states should be near 31475 cm^{-1}. As seen from Fig. 1, this places the $n_1=2$ states at the edge of the second-series ground state and are not observable in a crystal as thick as the one from which this absorption spectrum was obtained. Figure 2 however, shows both the absorption and reflection spectra of a crystal of slightly less than 1 μ thickness in the vicinity of the $n_2=1S$ state. In the spectra of this thinner crystal the $n_1=2$ states are clearly evident on the wings of $n_2=1S$ in both modes of observation.

If we are guided by the exciton spectra as seen in CdSe[3] and CdS,[9] the most plausible choice for the $n_1=3$ states is $3D_{\pm 2}$ and $3D_{\pm 1}$ as labeled in both Figs. 1 and 2. If we also take the $n_1=2$ states to be $2S$ and $2P_{\pm 1}$,

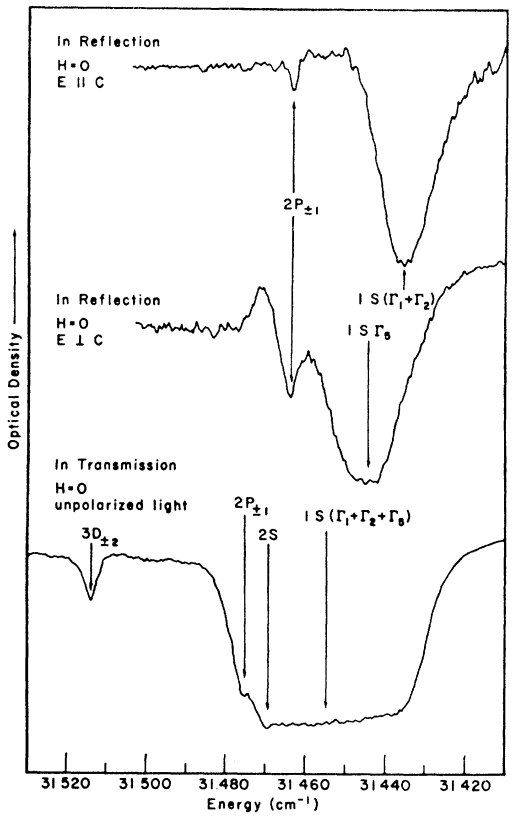

FIG. 2. Absorption and reflection spectra of a crystal of less than 1 μ thickness. The $2P_{\pm1}$ state of the first series is well defined in reflection as well as the ground states of the second series.

enough information is available to determine both the effective Rydberg and the anisotropy of this series. Using the second-order zero-field energies for the states as given in Table I, the parameters R_{eff} and α were obtained by a least-squares fitting of the calculated energies to those observed. The results of that fit are summarized in Table II.

Having obtained the effective Rydberg, one can calculate the x component of the exciton effective-mass tensor from Eq. (3). Using the values[13] $\epsilon=8.1$ and $\eta=1.1$, we find

$$\mu_x=0.16\pm0.02.$$

Effectively all the error in μ_x arises from the uncertainty in the dielectric parameters.

In addition to the parameter μ_x, we can also determine μ_x/μ_z, the exciton-mass anisotropy, from Eq. (4) and hence

$$\mu_x/\mu_z=0.59\pm0.05.$$

The $n_1=3$ and higher states of the first series as a function of magnetic field in the $\mathbf{H}\|C$ orientation are shown in Figs. 3 and 4 for two crystals of approximately

[13] Unfortunately the dielectric constants for hexagonal ZnS are not known. We have therefore used the cubic value of 8.1 determined by D. Berlincourt, H. Jaffe, and L. R. Shiozawa [Phys. Rev. **129**, 1009 (1963)] and have assumed $\eta=1.1$.

TABLE II. Summary of the zero-field data for the first (Γ_7-Γ_9) exciton series. $R_{\text{eff}}=247\pm2$ cm^{-1}; $\alpha=0.46\pm0.02$.

State	Observed energy (cm^{-1})	Calculated energy (cm^{-1})
$1S$	31 227.2	31 250.3
$2S$	31 469.6	31 469.8
$2P_{\pm1}$	31 475.2	31 474.7
$3D_{\pm1}$	31 509.5	31 509.1
$3D_{\pm2}$	31 513.5	31 513.5
$4F_{\pm2}$	31 525.6	31 525.3
5	31 532.0	31 533.1
Series limit	31 543±2	

2 and 5 μ thickness, respectively. The observed energies versus magnetic field for several crystal samples have been plotted in Fig. 5. Now this diagram contains a great deal of information, but for the present we confine our attention to those states which have been labeled $3D_{\pm2}$ and $3D_{\pm1}$.

From the observed diamagnetic shift of the $3D_{\pm2}$ state, the x component of the exciton effective-mass tensor can be obtained from (see Table I)

$$\mu_x=\left[\frac{1}{4}\left(\frac{e^2}{mc^2}\right)a_0^2\frac{1}{\sigma}\right]^{1/3}(\epsilon^2\eta)^{1/3}. \tag{8}$$

Since mixing via the quadratic field perturbation of the $3D_{\pm2}$ states with higher n states is significant, one cannot apply the first-order expression for the diamagnetic energy of the $3D_{\pm2}$ state as given in Table I to extract the quantity σ from the measured shift. As a first approximation we have considered the $n=3,4$ mixing

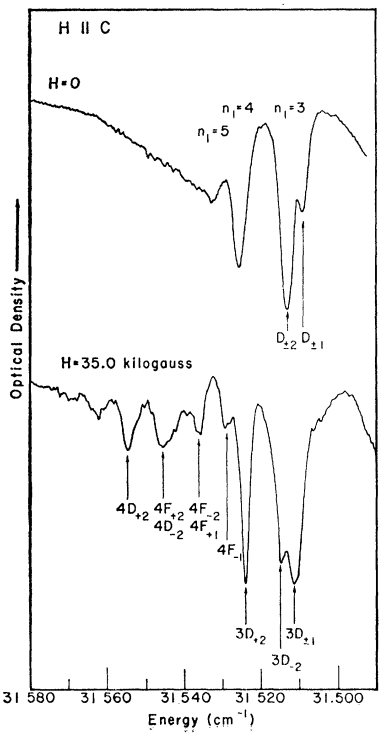

FIG. 3. Absorption spectra for a 2-μ-thick crystal in the vicinity of the $n_1=3$ states with the magnetic field parallel to the crystal C axis.

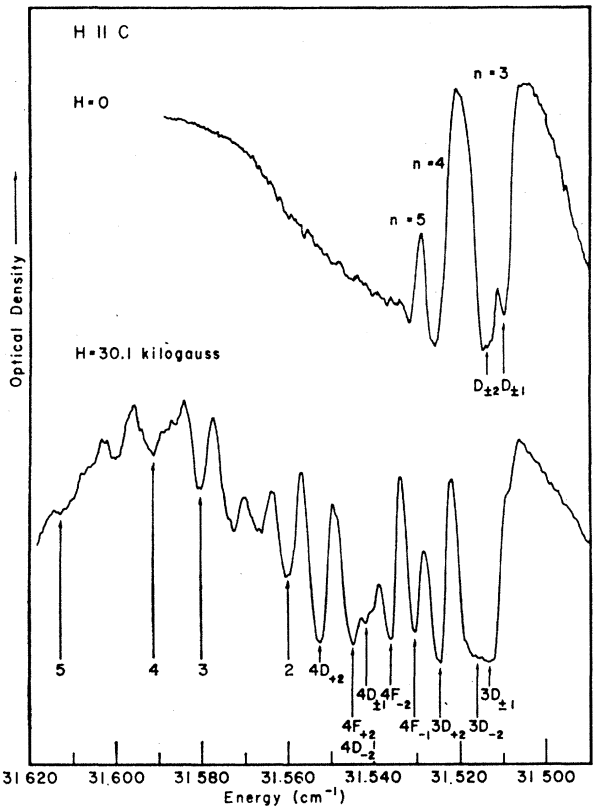

FIG. 4. Absorption spectra for a crystal of about 5 μ thickness in the vicinity of the $n_1=3$ states with the magnetic field parallel to the crystal C axis. Note the number of transitions above the series limit.

and adjusted the parameter σ to obtain a fit to the experimentally observed energies.

Having determined σ from the behavior of $3D_{\pm2}$, one can now plot the diamagnetic shift of the $3D_{\pm1}$ state and this has been done in Fig. 5. The $3D_{\pm1}$ state undergoes some broadening and the pair of lines plotted for this state represent the maximum linear splitting which would not result in an observable splitting.

The state identified as $2P_{\pm1}$ was also studied in transmission with $\mathbf{H}\|C$ and like $3D_{\pm1}$ does not split. In Fig. 6, both the experimentally observed energies versus magnetic field for this state and the first-order diamagnetic shift based on the value of σ found from $3D_{\pm2}$ have been plotted. For the $n_1=2$ states the higher state mixing can be safely neglected. The diamagnetic shift of this state as determined by a least-squares fit coincides with the predicted shift to within 10%. Here again a pair of lines has been plotted to represent the maximum linear splitting which would not result in an observable splitting. The agreement between the observed and theoretical energies based on our identification of the $3D_{\pm2}$, $3D_{\pm1}$, and $2P_{\pm1}$ states corroborates the assignment.

Using the appropriate values for ϵ and η, and the observed σ, we obtain

$$\mu_x=0.175\pm0.01.$$

The agreement between μ_x found from the diamagnetic shifts and that found from the effective Rydberg is excellent.

It should be noted that the parameter $\epsilon^2\eta$, which enters the calculation of μ_x from R_{eff} directly, enters the calculation of μ_x from the diamagnetic shift as the $\frac{1}{3}$ power, and hence this calculation is not as susceptible to error in $\epsilon^2\eta$.

Before considering the linear Zeeman splitting observed in $\mathbf{H}\|C$ we shall examine the $n_1=3$ states in the magnetic field orientation $\mathbf{H}\perp C$ since from the diamagnetic shifts in this case we can determine $(\mu_x/\mu_z)\sigma$ and hence μ_x/μ_z, and make a comparison with the zero-field value for this parameter. The absorption spectrum for a thin crystal with $H\perp C$ is shown in Fig. 7. In this geometry, the hole has no resolvable magnetic moment and all spin splitting is due to g_{ex} alone.[14]

The entire pattern in $H\perp C$ can be characterized by the two parameters $(\mu_x/\mu_z)\sigma$ and $\beta_0 a/\Delta_x$ representing

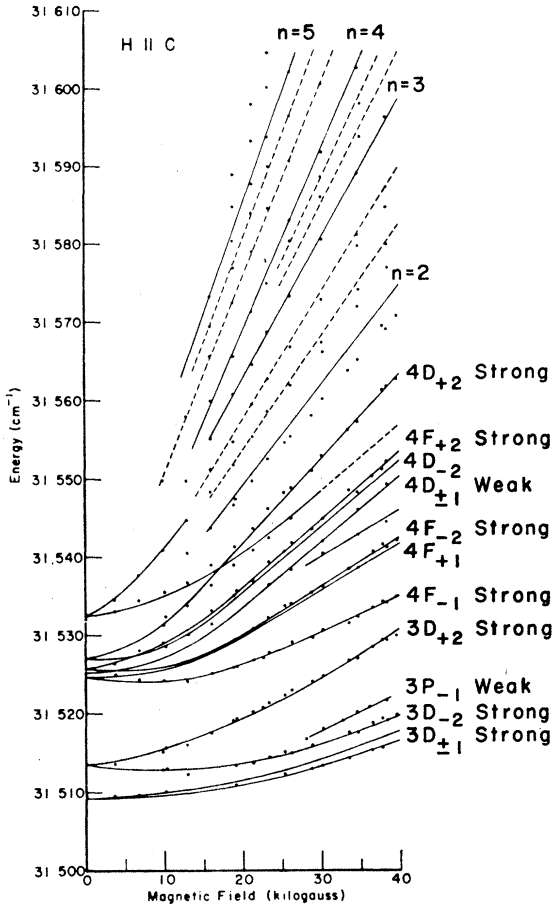

FIG. 5. The energies of the excited exciton states of the first series are plotted against magnetic field with the magnetic field parallel to the crystal C axis. Data from several crystal samples have been included.

[14] Since a magnetic field along x represents a perturbation of symmetry Γ_5, the hole in the Γ_9 valence band will have no resolvable magnetic moment since Γ_9 is not mixed with itself by a perturbation of Γ_5 symmetry.

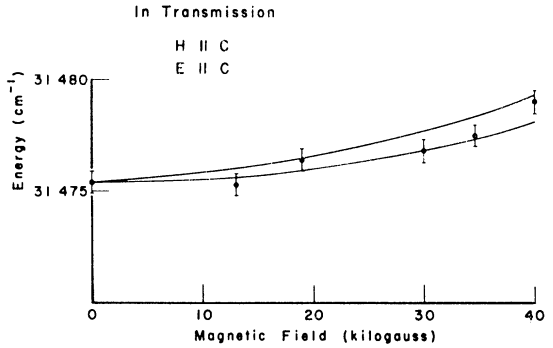

FIG. 6. Energy versus magnetic field for the $2P_{\pm1}$ state with the magnetic field parallel to the crystal C axis.

the effects of H_q and H_{lin}, respectively. Once again the interpretation of the diamagnetic shifts is complicated by mixing with higher n states through H_q, so as a first approximation we have considered only the $n=3,4$ mixing and diagonalized the resulting 12×12 secular determinant varying $(\mu_x/\mu_z)\sigma$ and $\beta_0 a/\Delta_x$ to obtain a fit to the experimental points. The best solutions have been plotted along with the experimental points in Fig. 8.

The two lowest states are the spin-split $3D_0$ and a spin-split component of $3D_{\pm1}$, while the highest state is a spin-split component of $3D_{\pm2}$. A linear spin-splitting corresponding to

$$|g_{ex}|=2.2\pm0.2$$

provides the best fit to these states. From the adjustment of the parameters $(\mu_x/\mu_z)\sigma$ and $\beta_0 a/\Delta_x$ we find

$$\mu_x/\mu_z=0.62\pm0.04.$$

The agreement between the exciton-mass anisotropy determined above and that obtained from the zero-field data is excellent. It should also be noted that whereas the zero-field determination required knowledge of the dielectric anisotropy, the value obtained here depends only on the ratio of the observed diamagnetic shift with $\mathbf{H}\perp C$ to that observed with $\mathbf{H}\|C$ and is independent of any dielectric constants.

From the theoretical fit one also obtains the quantity $\beta_0 a/\Delta_x$ which involves all the exciton-mass parameters. This quantity will be discussed again after we consider the linear effects for $\mathbf{H}\|C$.

In order to discuss the linear Zeeman effects in the orientation $\mathbf{H}\|C$, we must assign the proper symmetry to the observed states. In $H\perp C$, this was of no importance since the hole has no resolvable magnetic moment along x and only the electron spin produced splitting. In $H\|C$ however, both the electron and hole spin contribute to the linear splitting and we must know the symmetry of the observable states in order to determine the associated g value (see Table I).

In CdS,[9] states of both allowed symmetry $(\Gamma_1+\Gamma_2)$ and forbidden symmetry (Γ_5) were observed for $2P_{\pm1}$ in the polarization $\mathbf{E}\|C$ with the forbidden stronger than the allowed. For the $n_1=3$ states, a pair of lines was also observed which could be associated with $3D_{\pm2}$ $(\Gamma_1+\Gamma_2)$. Although no other $n_1=3$ states are identified as either allowed or forbidden, distinct intensity reversal effects were seen in the $H\perp C$ spectra of these states indicating the presence of forbidden transitions of some intensity.

As will be discussed in the conclusion of this paper, since the interband mixing is comparable for both CdS and ZnS and since the magnitude of the wave vector of the photon which induces transitions in ZnS is approximately a factor of 2 larger than that for CdS, we also assign Γ_5 or forbidden symmetry to the $2P_{\pm1}$ state in ZnS observed in the polarization $E\|C$. For the $n_1=3$ states in ZnS, we note from Fig. 7 that intensity changes upon reversal of the direction of the magnetic field for $H\perp C$ are almost nonexistent. This indicates, according to the analysis of Hopfield and Thomas,[9] that the observed transitions must be predominantly all allowed or all forbidden and not some combination of the two. It is easily shown that assignment of allowed symmetry to the observed $n_1=3$ states leads to a set of band parameters which are inconsistent with the observed behavior of the $n_1=2$ states and the magneto-optical effects to be discussed presently. We therefore assign Γ_5 symmetry to $3D_{\pm2}$, $3D_{\pm1}$ as well as to $2P_{\pm1}$ in order to obtain a consistent interpretation.

On this basis the linear splitting of the $3D_{\pm2}$ state yields the quantity (from Table I)

$$2/\Delta_x-\tfrac{1}{2}(g_{hz}-g_{ez})=3.0\pm0.1.$$

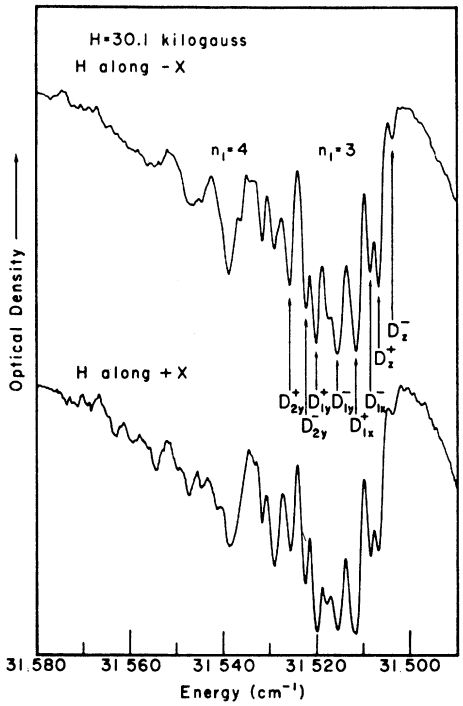

FIG. 7. Absorption spectra of a thin crystal with the magnetic field perpendicular to the crystal C axis for two directions of the magnetic field.

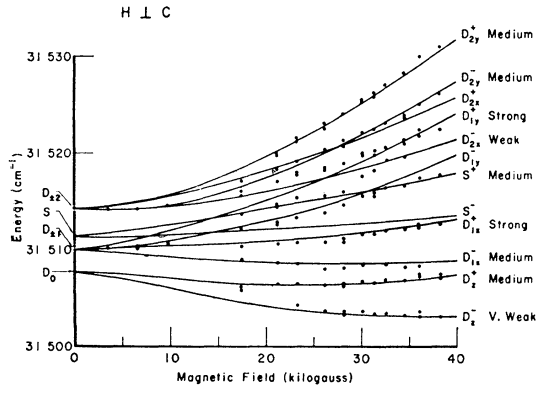

FIG. 8. The energies of the $n_1=3$ states plotted against magnetic field with the field perpendicular to the crystal C axis. Since no significant intensity reversals were observed, no distinction has been made between the data obtained from the two magnetic field directions. $D_z^{\pm}$ labels the spin-split components of $3D_0$ while $D^{\pm}_{1x}$, y represent the Zeeman and spin-split components of $3D_{\pm1}$ and $3D_{\pm2}$, respectively.

This is the value of the splitting actually plotted in Fig. 5. The $2P_{\pm1}$ and also the $3D_{\pm1}$ states do not split even at the largest magnetic fields used, although some broadening is detectable giving the quantity

$$1/\Delta_x-\tfrac{1}{2}(g_{hz}+g_{ez})=\pm0.3\pm0.1.$$

Again this is the splitting plotted in Figs. 5 and 6 for $3D_{\pm1}$ and $2P_{\pm1}$, respectively.

If either the sum or the difference of the g values was known then all the parameters involved in the splittings could be evaluated. The difference of the g values could be found from the linear splitting of either $3S\Gamma_5$ or $2S\Gamma_5$. Unfortunately, no $n_1=3$ state has been observed which could be identified as $3S\Gamma_5$. The $2S\Gamma_5$ state has been observed, however, on the very edge of the second-series ground state. Because of its position this line is barely visible although it does not appear to undergo any splitting in $\mathbf{H}\|C$ which indicates roughly that $g_{hz}\approx g_{ez}$.

The sum of the electron and hole g values could be obtained from the observation of the behavior of the $1S\Gamma_6$ state. This state represents the exciton triplet ground state with the electron and hole spins parallel. In $\mathbf{E}\|C$ it is a second-forbidden transition and observable only in very thick crystals. We have been unable to detect any absorption in the vicinity of the ground state which could be conclusively identified as $1S\Gamma_6$. Although we have no experimental values for the electron or hole g values in the z direction we can still interpret the $\mathbf{H}\|C$ splittings by drawing on the $\mathbf{k}\cdot\mathbf{p}$ perturbation predictions for ZnS and our observations of g_{ex} for $H\perp C$.

Roth[15] has shown that the electron g value in the Group II–VI compounds should be nearly isotropic and

$$g_e=2-\left(\frac{m}{m_e}-1\right)\frac{2E_{so}}{3E_g+2E_{so}}. \tag{9}$$

From this form we can draw a definite conclusion in regard to the electron g value. We see that for ZnS, where E_g (the direct band gap) is $\approx31\,540$ cm^{-1} and E_{so} (the spin-orbit splitting of the valence band) is ≈800 cm^{-1}, no reasonable value of m_e alters the fact that this expression gives an electron g value nearly equal to 2. Cardona[16] has also considered the question of the electron g value in ZnS taking into account the interaction of a higher lying conduction band. He finds a g value of about 1.8. In view of the fact that either approach indicates a g value for the conduction electron of about 2, we will assume that

$$g_{ez}=1.9\pm0.1.$$

As mentioned earlier, the observed spin-splitting in $H\perp C$ yielded a value of $|g_{ex}|=2.2\pm0.2$. Since some anisotropy is no doubt present in g_e for hexagonal ZnS, this result is in agreement with the $\mathbf{k}\cdot\mathbf{p}$ prediction.

If we use the above value of g_{ez} in the $2P_{\pm1}$, $3D_{\pm1}$, and $3D_{\pm2}$ splittings we find two possibilities for the parameters $1/\Delta_x$ and g_{hz}, namely,

$$1/\Delta_x=1.5\pm0.3,\quad 1/\Delta_x=0.8\pm0.3;$$
$$g_{hz}=1.5\pm0.8,\qquad g_{hz}=-0.9\pm0.8.$$

The ambiguity arises because we do not know the sign of the small quantity $1/\Delta_x-\frac{1}{2}(g_{hz}+g_{ez})$ and the large error in g_{hz} is simply due to the accumulated errors in g_{ez} and the linear splittings. There are however, indications that the pair associated with a positive-hole g value of ≈1.5 is the best choice.

First, we have observed $2S\Gamma_5$ in transmission and it does not appear to undergo the splitting necessary for $g_{hz}=-0.9\pm0.8$ or $-(g_{hz}-g_{ez})>2$.

Second, some recent work on the Faraday rotation in cubic ZnS[17] indicates that (g_h+g_e) lies between three and four. While one expects the hole mass and g value to be different for the two structures, the differences are not so great as to change the rough estimate of (g_h+g_e).

Finally, the choice of $(g_{hz}-g_{ez})$ nearly equal to zero will allow us to interpret the absorption spectra observed above the band gap as shown in Figs. 4 and 5.

We are now in a position to evaluate all the effective-mass parameters. Using the value of $1/\mu_x$ obtained from the $H\|C$ diamagnetic shifts, and the value of $1/\Delta_x$ associated with the positive-hole g value, we find

$$m_{ex}=0.28\pm0.03,$$
$$m_{hx}=0.49\pm0.06,$$

where m_e and m_h are in terms of the free-electron mass. From the $\mathbf{H}\perp C$ diamagnetic shifts we were able to determine μ_x/μ_z and having $1/\mu_x$ we find

$$1/\mu_z=3.5\pm0.3.$$

[15] L. Roth, Phys. Rev. **118**, 1534 (1960).

[16] M. Cardona, J. Phys. Chem. Solids **24**, 1543 (1963).

[17] A. Ebina, T. Koda, and S. Shionoya, ISSP Technical Report, 1965 (unpublished).

The value of $1/\Delta_z$ can be obtained from the splitting term $\beta_0 a/\Delta_x$ determined from $\mathbf{H}\perp C$ using Eq. (6). We find

$$1/\Delta_z = 4.0 \pm 1.0.$$

Unfortunately a large error arises here because of the accumulated errors in $1/\Delta_x$, μ_x/μ_z, and a which are used to calculate $1/\Delta_z$. Nevertheless, with the above values we obtain

$$m_{ez} = 0.27 \pm 0.04, \quad |m_{hz}| > 1.$$

The ambiguity in the sign and magnitude of m_{hz} is due to the large error present in $1/\Delta_z$. For the electron-mass values we note that within the experimental error, the electron mass is isotropic, $m_{ex} = m_{ez}$.

So far in our analysis of the linear splittings of the $n_1 = 2,3$ states we have neglected any effects arising from the finite wave vector of the exciton. In the orientation $\mathbf{H}\|C$ a term appears in the Hamiltonian (1) which has the form[9,3]

$$\tfrac{1}{2}(\beta_0/\mu_x) K_y x H_z, \tag{10}$$

where K_y is the exciton or incident-photon wave vector. Since this additional perturbation depends on matrix elements of the operator x, it is similar to an electric field normal to the direction of motion of the exciton and the magnetic field. The effect of this quasielectric field is to alter the observed Zeeman splittings. Estimates of the effect of this perturbation on the band parameters have been made and it is found that the value of $1/\Delta_x$ determined from the linear splittings of the $3D_{\pm 2}$ and $3D_{\pm 1}$ states is decreased by approximately 10%. In view of this, the value given for $1/\Delta_x$ has been corrected by this amount.

Although we are able to adequately treat the $n_1 = 2,3$ states in terms of the exciton Hamiltonian (1) by considering the magnetic field to be small, we cannot handle the $n_1 = 4$ states in the same manner. At high fields most of the states are above the band gap and are in a region where the magnetic energy is comparable to the Coulomb binding energy, so that the magnetic field cannot be considered as a perturbation. Furthermore, some of the $n_1 = 5$ states overlap the $n_1 = 4$ as seen in Fig. 5, and the mixing through H_q is then very pronounced even at low fields. Unfortunately, the magnetic field is not large enough for us to apply any form of high magnetic field approximation. Nevertheless, the behavior of the $n_1 = 4$ states can be interpreted qualitatively on the basis of approximate diamagnetic shifts at lower fields and linear splittings.

Neglecting quasielectric field effects, m will be a good quantum number for all magnetic fields and we should observe two pairs of states with splitting approximately equal to that of $3D_{\pm 2}$ and two states with splitting approximately equal to that of $3D_{\pm 1}$. In addition, the possibility that states of allowed symmetry may also be present should not be excluded. The curves plotted for the $n_1 = 4$ states in Fig. 5 consist of the calculated first-order diamagnetic shifts for forbidden $4F_{\pm 2}$, $4D_{\pm 2}$, and $4D_{\pm 1}$ at low fields with the appropriate linear splittings preserved during a straight-line extrapolation to high fields. The $4F_{\pm 1}$ state must be treated to second order since it is mixed with $4P_{\pm 1}$ by the anisotropy and H_q. For this state, the low-field diamagnetic shift indicates that the lowest $n_1 = 4$ states observed may be associated with $F_{\pm 1}$ allowed and the linear splitting appropriate for this state has been plotted in Fig. 5. Our interpretation of the $n_1 = 3$ states as $3D_{\pm 2}$ and $3D_{\pm 1}$ thus allows us to account for the behavior of the $n_1 = 4$ states quite well.

For the states above $n_1 = 4$ we may apply the high-field exciton approximation developed by Elliot and Loudon.[4,5] As shown in Fig. 5 for $\mathbf{H}\|C$, a large number of absorption lines are observed above the series limit at high magnetic fields. For these states the magnetic energies are at least an order of magnitude greater than the Coulomb binding energies of the exciton states from which they arise, and it should be possible to treat these states approximately by assuming the limit of infinite magnetic field but nonvanishing Coulomb interaction. In this case the exciton energy levels at high fields are given by

$$E = \frac{eHH_z}{m_{ex}c}(n_e + \tfrac{1}{2}) + \frac{eHH_z}{m_{hx}c}(n_h + \tfrac{1}{2}) \pm \tfrac{1}{2}(g_{hz} \pm g_{ez})\beta_0 H_z - (R/\nu^2). \tag{11}$$

To avoid the complications due to the Coulomb term R/ν^2 we consider only the magnetic field dependence and examine the slopes of the magnetic levels.

In order to interpret the observed absorption on the basis of this model we make use of the fact that the total electron-hole wave function, which is a product of the band wave functions and a spatial part derived from solutions of the Hamiltonian (1) with the Coulomb dependence omitted, has a symmetry determined only by the band symmetries at $\mathbf{k} = 0$, or $\Gamma_5 + \Gamma_6$ for an electron in a Γ_7 conduction band and a hole in a Γ_9 valence band. Since states with symmetry Γ_5 correspond to first-forbidden transitions while states with symmetry Γ_6 correspond to weaker second-forbidden transitions, we assign Γ_5 symmetry to the states observed above the series limit. For states of symmetry Γ_5 the total g value $(g_{hz} - g_{ez})$ is nearly zero. If we now admit the selection rule on n_e and n_h that $\Delta n = 0$, the energy as a function of H becomes

$$dE/dH \cong (\beta_0/\mu_x)(2n+1) \tag{12}$$

and the observable Landau states should have slopes which depend only on $1/\mu_x$ and the quantum number n. Using the value of μ_x obtained from the preceeding exciton analysis, lines for $n = 2, 3, 4$, and 5 have been plotted in Fig. 5 and agree very well with the experimentally observed slopes.

The transitions for which $n_e=n_h$ do not account for all the observed absorption lines however, there being in general two weaker lines lying between each of the allowed ones. If we now admit the selection rule $\Delta n=\pm 1$, the slopes of the Landau lines depend on both $1/\mu_x$ and $1/\Delta_x$. Calculating the slopes of these transitions, we find agreement with all of the observed absorption lines.

In addition to interpreting the high-field absorptions in $H\|C$, we can carry out an identical analysis for $H\perp C$. In Fig. 9 we have plotted the experimental energies versus magnetic field in the $H\perp C$ orientation. In this orientation the field dependence of the Landau levels is given by[18]

$$\frac{dE}{dH}=\frac{e\hbar}{m_e'c}(n_e+\tfrac{1}{2})+\frac{e\hbar}{m_h'c}(n_h+\tfrac{1}{2})\pm\tfrac{1}{2}g_{ex}\beta_0, \quad (13)$$

where $1/m_e'$ and $1/m_h'$ are defined as

$$\frac{1}{m_e'}=\frac{1}{(m_{ex}m_{ez})^{1/2}}, \quad \frac{1}{m_h'}=\frac{1}{(m_{hx}m_{hz})^{1/2}}. \quad (14)$$

Unfortunately we cannot directly fit the observed slopes with the expression above because of the large uncertainty in the value of m_{hz} determined from the exciton analysis. However, if we make the educated guess that the uppermost line is probably associated with n_e, $n_h=4$ we can use the experimentally determined mean slope of this split line to evaluate m_{hz}, using the known values of m_{ex}, m_{ez}, and m_{hx}. In this way we find

$$|m_{hz}|\sim 1.4.$$

We are now in a position to calculate the slope of the n_e, $n_h=3$ state and we find that there is indeed another absorption line lower in energy which has a field dependence appropriate to an $n=3$ state. As in the $H\|C$ orientation there are additional lines between the $n=3,4$. Once again admitting the selection rule $\Delta n=\pm 1$ we can calculate the dependence for these transitions and make a comparison with experiment. In Fig. 9 we have plotted lines for both $\Delta n=0$ and $\Delta n=\pm 1$ transitions with a spin splitting equal to $|g_{ex}|=2.0$. The actual spin splitting appears to be somewhat smaller than that for $|g_{ex}|=2.0$, but in view of the fact that the lines have not been well resolved, the difference is within the experimental error. The agreement between the observed field dependence of the Landau states based on the identification of the $n=4$ state is quite good, and in fact no other identification of the states fits as well.

While analysis of the first-series absorption spectra yields a complete set of electron and hole parameters, this is unfortunately not the case for the second series. Even in the best crystals available, the widths of the

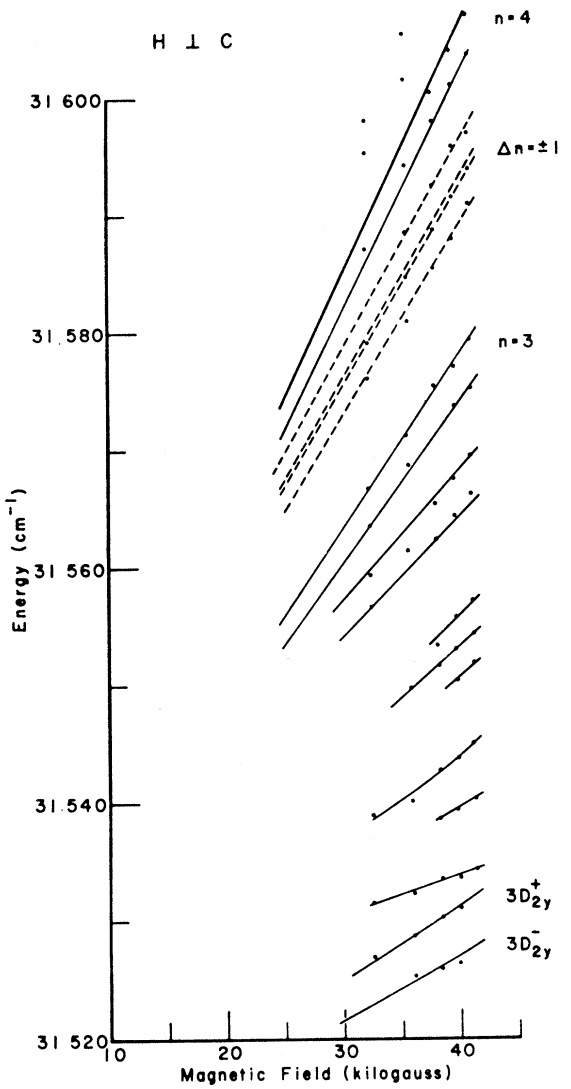

FIG. 9. Energy versus magnetic field for a crystal of approximately 5 μ thickness with the magnetic field perpendicular to the crystal C axis. The Landau states and a component of the $3D$ state are shown.

$n_2=2,3$ states are much greater than the corresponding first-series states as can be seen in Fig. 1. Furthermore, since the second series arises from a Γ_7 conduction band and a Γ_7 valence band, all the $n_2=2$ states are observable with $E\|C$, i.e., there are $2S$, $2P_0$, and $2P_{\pm 1}$ states allowed symmetry $\Gamma_1+\Gamma_2$, and because of the intrinsic linewidths no anisotropy splitting is seen. The problem is even further complicated if we include the possibility of forbidden states as well.

Because of the band symmetries, the situation is also somewhat different for the $n_2=3$ states. There is now no allowed $D_{\pm 2}$ state observable with $E\|C$ since a $D_{\pm 2}$ state for a $\Gamma_7-\Gamma_7$ exciton has symmetry $\Gamma_3+\Gamma_4+\Gamma_5+2\Gamma_6$ although transitions to forbidden $D_{\pm 2}$ may occur. The $n_2=3$ state at zero field therefore consists of a $3P_{\pm 1}$, $3D_{\pm 1}$ and perhaps a forbidden $3D_{\pm 2}$ state unresolved because

[18] W. Shockley, Phys. Rev. **90**, 491 (1953).

TABLE III. Summary of the zero-field data for the second (Γ_7-Γ_9) exciton series.

State	Observed energies (cm^{-1})
1	31 455
2	31 702
3	31 745
Assuming $\alpha=0.45$,	$R_{eff}=275\pm10$ cm^{-1}.
Series limit	$31\,780\pm10$ cm^{-1}.
Using $\epsilon=8.1$,	$\eta=1.1$, $\mu_x\sim0.18$.

of the intrinsic linewidth. On this basis and assuming an anisotropy equal to that found for the first series one can calculate approximately the effective Rydberg and series limit, and using the value of $\epsilon^2\eta$, determine μ_x. These results are summarized in Table III. From the series limits for both the first and second series we find the crystal-field splitting of the $\Gamma_9-\Gamma_7$ valence band to be 240 ± 10 cm^{-1}.

DISCUSSION

Let us review the experimental results for the first series. Identification of the $n_1=3$ states as $3D_{\pm1}$, $3D_{\pm2}$ and the $n_1=2$ state seen in transmission as $2P_{\pm1}$ has allowed us to evaluate the reduced effective mass of the exciton from both the zero-field positions of the absorptions and the diamagnetic shift of the $3D_{\pm2}$ state. The agreement between the value of μ_x obtained in both ways is excellent considering the uncertainty in $\epsilon^2\eta$. Furthermore, the predicted diamagnetic shift of the $2P_{\pm1}$ state based on the observed shifts of $3D_{\pm2}$ and $3D_{\pm1}$ accounts for the behavior of this state to within 10%, so had we originally based our evaluation of μ_x on the $n_1=2$ state rather than $n_1=3$, the result would still agree with that obtained from the effective Rydberg. This is an important point since it could be argued that the effects of higher state mixing and quasielectric field effects could alter the diamagnetic shifts of the $n_1=3$ states. For the $n_1=2$ states however, these effects are negligible.

With the magnetic field perpendicular to the crystal C axis, we have been able to fit the observed absorption lines for the $n_1=3$ states quite well and obtained the value of μ_x/μ_z by comparing the diamagnetic shifts in the two orientations $H\perp C$ and $H\|C$. The agreement between μ_x/μ_z obtained in this way with the value calculated from the anisotropy splitting, based on the identification of the $n_1=3$ states as $3D_{\pm1}$, $3D_{\pm2}$, is also excellent considering the uncertainty in the dielectric anisotropy.

By assigning the forbidden symmetry Γ_5 to the states seen in transmission and assuming $g_{ez}=1.9\pm0.1$, the linear splitting of the $n_1=2,3$ states allowed us to evaluate the parameter $1/\Delta_x$ and hence both m_{ex} and m_{hx} using the value of $1/\mu_x$.

From the linear splitting in the orientation $H\perp C$ we directly obtained the electron g value along x and found it to be nearly equal to 2. The splitting parameter a was also determined and allowed evaluation of $1/\Delta_z$. When this quantity was combined with $1/\mu_z$ we found that $m_{ex}=m_{ez}$ within the experimental error and this result is in agreement with elementary $\mathbf{k}\cdot\mathbf{p}$ predictions for the hexagonal Group II–VI compounds.

Although the $n_1=4$ states could not be treated exactly, the observed behavior at high fields could be well accounted for in terms of the splittings associated with both forbidden and allowed transitions and approximate diamagnetic shifts.

Finally, using the data obtained from the low-lying excited exciton states we were able to interpret the absorptions seen far above the band gap in terms of the high magnetic field or Landau approximation for both the $H\|C$ and $H\perp C$ orientations. While the Landau data for $H\|C$ did not yield any additional information, interpretation of the $H\perp C$ data gave an approximate value for m_{hz}.

The most interesting feature of the exciton spectra in ZnS is that interpretation of the excited states in terms of the intensity reversal effects and the requirement for internal consistency forces the assignment of forbidden symmetry to the observed $n_1=2,3$ states. The occurrence of very strong forbidden transitions in ZnS can however be accounted for on the basis of the interband mixing. It has been shown[7] that the interband mixing and the presence of strong forbidden transitions in the Group II–VI compounds are closely related so that in a sense the interband mixing can be used as a measure of the relative strengths of the allowed and forbidden transitions.

In CdS [9] it was observed that for the $2P_{\pm1}$ states the ratio of the forbidden and allowed intensities was about 8 to 5. The magnitude of the photon wave vector producing optical transitions in ZnS turns out to be about twice that for CdS. Since the interband mixing is comparable in both CdS and ZnS and the forbidden transitions have intensity proportional to K^2, then to a first approximation one should indeed expect to see forbidden $2P$ transitions a factor of ≈6 stronger than the allowed in ZnS.

For CdSe on the other hand, no forbidden transitions were detected in the polarization $E\|C$ although their presence was indicated by intensity reversal effects. In view of the discussion just given for CdS and ZnS this is not surprising. Recall that the interband mixing for CdSe is down by a factor of about $\frac{1}{4}$ from that for either CdS or ZnS. The wave vector for transitions in CdSe is about $\frac{2}{3}$ of that for CdS so that to a first approximation the forbidden transitions should have intensity about $\frac{1}{5}$ that of the allowed and this is indeed in qualitative agreement with the observed behavior of CdSe.

We see then that the occurrence of strong forbidden transitions is in line with the trend exhibited by the exciton spectra in CdSe and CdS. While we expect the forbidden transitions for the $n=2$ states to swamp those allowed in ZnS, it is surprising that the observed $3D$

states are also forbidden. Whether or not ZnS represents an unusual case could be decided experimentally by a more careful analysis of the $n_1=3$ states in both CdSe and CdS.

At present there are no reliable experimental mass values for ZnS with which we can compare our results. Estimates of the effective electron mass using standard $\mathbf{k}\cdot\mathbf{p}$ perturbation theory have been made however, by ourselves and Cardona.[16] In the latter calculation the effect of a higher conduction band on the electron effective mass was considered, and a value of $m_e=0.39$ was found. Now this is to be compared with $m_e=0.28$ as found in this series of experiments. The discrepancy of about 25% may be due to a combination of factors. First there is the inherent error of at least 10% in our determination of the electron mass. Secondly, we have neglected the effects of the interband mixing on the exciton Hamiltonian and evaluated the band parameters in terms of a simple single-conduction-band–single-valence-band model. Finally, there exists the possibility that the interband matrix elements involved in the $\mathbf{k}\cdot\mathbf{p}$ estimates of the electron effective mass may not be equal for all the Group II–VI compounds. Considering these factors, we believe that no definite conclusions can be drawn from the discrepancy between our measured electron mass and the calculated value.

PHYSICAL REVIEW VOLUME 153, NUMBER 3 15 JANUARY 1967

Lattice Dynamics of Sodium Fluoride

W. J. L. BUYERS*
Chalk River Nuclear Laboratories, Atomic Energy of Canada Limited, Chalk River, Ontario, Canada
(Received 8 August 1966)

Phonons in sodium fluoride have been studied at room temperature using inelastic neutron scattering techniques. Consistent results were obtained using a cold neutron time-of-flight apparatus and a triple-axis spectrometer. The time-of-flight results were interpolated on to symmetry directions from the observed scattering surfaces. The frequencies in units of 10^{12} sec^{-1} of some typical phonons are: TA(0,0,1), $\nu=4.39\pm0.04$; LO(0,0,0.984), $\nu=8.52\pm0.15$; LA(0,0,0.972), $\nu=7.94\pm0.18$; TO(0.488, 0.488, 0.488), $\nu=6.19\pm0.07$. The optical branches extrapolated to small wave vector are in agreement with the infrared absorption frequency and the Lyddane-Sachs-Teller relation. Hardy and Karo's deformation-dipole model is in agreement with the results to within 6%, but the rigid-ion model differs by as much as 19%. The results are well fitted by a shell model containing nine parameters in which the ionic charge is 0.91.

1. INTRODUCTION

ALKALI halides have been the subject of many theoretical and experimental investigations of the dispersion relation for vibrational modes. Models of the solid have been developed which facilitate the calculation of dispersion relations without recourse to consideration of the fundamental theory underlying the atomic interactions. The extremely simple Born-Mayer model used by Kellerman[1] was very successful in describing the specific heat, while the various versions of the theory in the dipole approximation, reviewed by Cochran,[2] are able to resolve difficulties in the optical and dielectric behavior of the solid that existed in the earlier work. The most complete confirmation of the reliability of a particular model has been carried out on NaI and KBr by neutron spectroscopy,[3] while NaCl has been the subject of a recent x-ray investigation.[4] It was found in these studies that a general description of the observed dispersion relations was obtained when models such as the simple shell model[5] or the deformation-dipole model,[6] whose parameters were fitted to long-wavelength data, were compared with the scattering results. If, on the other hand, a model was fitted to the observed frequencies, much better agreement could be obtained, often within the experimental accuracy, but only at the expense of losing the simple picture given by the model.[3]

In NaI, NaCl, and KBr, the polarizability of the crystal is higher than the average for alkali halides, and the crystal polarizability[7] of the negative ion is considerably greater than that of the positive ion. It is therefore of interest to see if, in a crystal of low polarizability, whose ions are comparable in size, the simple version of the theory for alkali halides is more satisfactory. Sodium fluoride is well suited for this study. It was also chosen because it has favorable properties for x-ray as well as neutron scattering, and could thus

* Part of this work was performed at the Department of of Natural Philosophy, University of Aberdeen, Scotland.

[1] E. W. Kellerman, Phil. Trans. Roy. Soc. **A238**, 513 (1940).

[2] W. Cochran, in *Lattice Dynamics*, edited by R. F. Wallis (Pergamon Press, Inc., New York, 1965).

[3] R. A. Cowley, W. Cochran, B. N. Brockhouse, and A. D. B. Woods, Phys. Rev. **131**, 1030 (1963); A. D. B. Woods, W. Cochran, and B. N. Brockhouse, *ibid.* **119**, 980 (1960).

[4] W. J. L. Buyers and T. Smith, Phys. Rev. **150**, 758 (1966).

[5] W. Cochran, Phil. Mag. **5**, 1082 (1959).

[6] A. M. Karo and J. R. Hardy, Phys. Rev. **129**, 2024 (1963).

[7] J. Tessman, A. Kahn, and W. Shockley, Phys. Rev. **92**, 890 (1953).